ChemComm

COMMUNICATION

Published on 17 August 2026

Cite this: DOI: 10.1039/d6cc04776a

Received 19th July 2026,
Accepted 16th August 2026

DOI: 10.1039/d6cc04776a

rsc.li/chemcomm

Single-atom Ni catalysis accelerates desolvation for high performance Zn–MnO_2 batteries

Peng Chen,[ab] Renyou Zhou,[a] Enqi Zhai,[a] Jinyuan Zhao,[c] Jing Zhang,[d] Xue Zhang,[e] Jian Wang *[fgh] and Yongzheng Zhang *[a]

The $Zn(solvents)_x^{2+}$, with high desolvation energy barriers, leads to the formation of H^+ and partial desolvated Zn^{2+} simultaneously intercalated into the MnO_2 cathode. A single-atom Ni catalyst on nitrogen-doped carbon (SANi-NC) is introduced to achieve stepwise atom-level catalytic desolvation of $Zn(H_2O)_x^{2+}$, which enables more insertion of Zn^{2+}, thereby achieving high-performance Zn–MnO_2 batteries.

Aqueous Zn metal batteries are regarded as promising next-generation energy storage systems due to their inherent safety and low cost, with the Zn anode delivering a high theoretical capacity of 820 mAh g^{-1} *via* two-electron redox reactions.[1–3] Among various cathodes, MnO_2 is particularly attractive due to its spacious tunnel structure and expected two-electron Mn^{4+}/Mn^{2+} capacity of 616 mAh g^{-1}.[4] However, its practical performance is severely constrained by several tough issues. The sluggish transport and high desolvation barriers of $Zn(H_2O)_6^{2+}$ lead to accumulation of incompletely desolvated species and massive free active H_2O at the MnO_2 cathode–electrolyte interface.[5–7] In addition, the competitive co-intercalation of partially desolvated $Zn(H_2O)_x^{2+}$ and H^+ reduces the reactive sites and shifts the redox from two-electron (616 mAh g^{-1}) to single-electron Mn^{4+}/Mn^{3+} (308 mAh g^{-1}, Fig. 1a).[8,9] Moreover, the accompanying intercalation/deintercalation of $Zn(H_2O)_x^{2+}$ and H^+ also induce lattice distortion of MnO_2, further accelerating Mn^{n+} dissolution and deteriorating battery performance.[10–12]

To address these challenges, electrolyte engineering has been widely employed to weaken Zn^{2+}–H_2O interactions and reconstruct the solvation structure.[13–15] While this approach reduces the desolvation barrier of $Zn(H_2O)_6^{2+}$ and liberates more free Zn^{2+}, the strong coordination between electrolyte additives and Zn^{2+} creates a new desolvation penalty. Moreover, parasitic reactions with the Zn anode further compromise battery performance.[16] An alternative strategy is catalytic engineering, which introduces electrocatalysts at the cathode–electrolyte interface to regulate interfacial ionic kinetics. In our previous work, we proposed a stepwise catalytic desolvation strategy in which electrocatalysts form strong interactions with H_2O to weaken Zn^{2+}–H_2O bonding and lower the desolvation barrier, aiming at rapid interfacial charge transport, fast Zn^{2+} diffusion and H_2O-free intercalation.[17–19] However, conventional electrocatalysts often suffer from insufficient catalytic activity and underutilized active sites.[20,21]

Single-atom catalysts (SACs) offer compelling advantages in this regard, exhibiting 100% atomic utilization and facile synthesis.[22] They can anchor H_2O *via* strong orbital interactions between central metal orbitals and O atoms, as well as between coordinated N and H atoms, thereby restricting interfacial H_2O migration.[23] Meanwhile, orbital hybridization

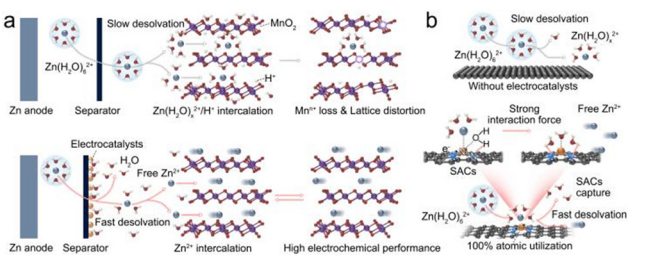

Fig. 1 (a) Mechanism diagram illustrating the effect of $Zn(H_2O)_6^{2+}$ on MnO_2 cathodes without/with electrocatalysts. (b) Schematic mechanism of atomic-level tandem catalytic desolvation enabled by SACs.

[a] School of Textile and Clothing, Nantong University, Nantong, 226019, China. E-mail: zhangyongzheng@ntu.edu.cn
[b] Institute for Innovative Materials and Energy, Faculty of Chemistry and Chemical Engineering, Yangzhou University, Yangzhou, 225002, China
[c] School of Pharmacy, Nantong University, Nantong, 226019, China
[d] School of Materials Science and Engineering, Xi'an University of Technology, Xi'an, 710048, China
[e] Institute for Experimental Molecular Imaging, Faculty of Medicine, RWTH Aachen University, 52074, Aachen, Germany
[f] Helmholtz Institute Ulm (HIU), Ulm, D89081, Germany
[g] Karlsruhe Institute of Technology (KIT), Karlsruhe, D76021, Germany. E-mail: jian.wang@kit.edu
[h] i-Lab & CAS Key Laboratory of Nanophotonic Materials and Devices, Suzhou Institute of Nano-Tech and Nano-Bionics, Chinese Academy of Sciences, Suzhou, 215123, China

between central metal sites and Zn species accelerates interfacial charge transfer, enabling rapid desolvation and endowing Zn‖MnO_2 batteries with satisfactory long-term cycling stability.[24,25] Therefore, it is of significance to construct interfacial atomic catalysts to accelerate the formation of free Zn^{2+} at the cathode interface.

In this work, Ni single atoms (SANi) are initially immobilized on N-doped carbon (Fig. 1b), working as a functional glass fiber separator (SANi-NC@GF). Theoretical calculations reveal that the introduced SANi anchors H_2O with a strong binding energy of 0.17 eV, disrupting the solvation structure of $Zn(H_2O)_6^{2+}$ and accelerating the desolvation barrier from 2.56 eV to 1.80 eV. Benefiting from the synergistic effect of highly active SANi sites and the fast electron transport of N-doped carbon, fast Zn^{2+} migration is achieved. Consequently, the Zn|SANi-NC@GF|MnO_2 full cell delivers a high specific capacity of 414.5 mAh g^{-1} after 180 cycles under a current density of 0.5 A g^{-1}.

As shown in Fig. 2a, high-density isolated Ni atoms are uniformly dispersed on the surface of NC, confirming the successful fabrication of SANi-NC. Elemental mappings further verify the homogeneous distribution of C, N and Ni (Fig. 2b). X-ray photoelectron spectroscopy (XPS) corroborates the presence of C, N and Ni, while the weak Ni signal originates from the Ni atom loading content (Fig. 2c, d and Fig. S1). Owing to the coordination between Ni and N atoms, Ni loses electrons and presents an elevated valence state (Ni $2p_{3/2}$, 855.1 eV). Meanwhile, the N 1s spectrum is deconvoluted into graphitic N, pyrrolic N, pyridinic N, and Ni–N peaks, demonstrating that Ni atoms are doped into the carbon framework and bonded with N configurations (Fig. 2d).[26–28] Additionally, abundant N active sites coupled with SANi synergistically anchor H_2O through hydrogen bonds and the empty 3d orbitals of the central Ni atoms. Synchrotron X-ray absorption spectroscopy (XAS) was utilized to further investigate the chemical environment of Ni in SANi-NC. As shown in Fig. 2e and f, partial electrons of Ni are captured by N, leading to an intermediate oxidation state of Ni between Ni^0 and Ni^{2+}, which is consistent with the XPS results. Moreover, a fitted peak located at approximately 1.71 Å is observed, which is ascribed to the Ni–N bond.[29,30] Furthermore, no other distinct Ni–Ni bonding signal is detected, further verifying that Ni atoms exist exclusively as isolated single atoms.

Subsequently, a theoretical model of SANi-NC was constructed based on the XAS and XPS results. A series of adsorption energies toward H_2O and Zn species, as well as desolvation energy barriers of $Zn(H_2O)_6^{2+}$, were obtained. As shown in Fig. 3a, benefiting from the synergistic effect of the unsaturated Ni atom and coordinated N atoms, the adsorption energy of H_2O on SANi-NC (0.17 eV) is stronger than that on NC (0.09 eV). Meanwhile, 3d orbital hybridization between Ni and Zn enables stronger adsorption of Zn on SANi-NC (−0.28 eV) compared with NC (−0.21 eV), suggesting that the Ni atomic sites can immobilize $Zn(H_2O)_6^{2+}$ and further accelerate the subsequent desolvation process (Fig. 3b).[31] Then, the desolvation energy barriers of $Zn(H_2O)_6^{2+}$ on SANi-NC and NC substrates were calculated. Owing to the strong adsorption capacity of SANi-NC toward both H_2O and Zn^{2+}, $Zn(H_2O)_6^{2+}$ can be firmly captured. Combined with the continuous electron transport network of NC, a low desolvation barrier of 1.80 eV is achieved on SANi-NC (Fig. 3c and Fig. S2). In contrast, the limited active sites on bare NC lead to a higher desolvation barrier of 2.56 eV. Incomplete interfacial desolvation leaves abundant active H_2O, which triggers severe interfacial side reactions and restricts the redox process to the single-electron Mn^{4+}/Mn^{3+} pathway.[32] Accordingly, the migration energy barrier of interfacial Zn^{2+} was also compared. The introduction of low-electronegativity Ni atoms, with abundant free electrons, increases the free electron density in SANi-NC and expands the delocalized charge distribution, simultaneously lowering both the desolvation barrier and migration energy barrier (0.06 eV, Fig. 3d).[33] In contrast, the sparsely distributed N dopants on bare NC act as electron traps and hinder Zn^0 diffusion, corresponding to a higher diffusion barrier of 0.11 eV (Fig. 3d and Fig. S3, S4). Thus, Ni atoms anchor H_2O to weaken the Zn^{2+}–H_2O bonding interaction

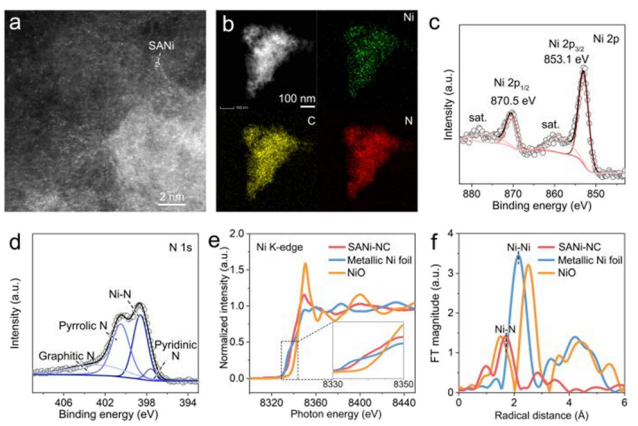

Fig. 2 (a) High-angle annular dark-field scanning transmission electron microscopy (HAADF-STEM) images. (b) The corresponding element mapping images. XPS spectra of (c) Ni 2p and (d) N 1s. (e) FT-EXAFS curves and (f) fitting curves of SANi-NC, Ni foil and NiO.

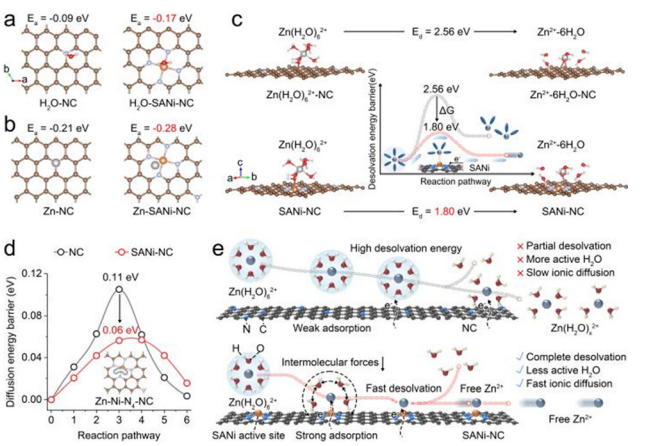

Fig. 3 The adsorption energy of (a) H_2O and (b) Zn, (c) desolvation energy barrier of $Zn(H_2O)_6^{2+}$, and (d) diffusion energy barrier of Zn on NC with/without SANi. (e) Schematic diagram of fast $Zn(H_2O)_6^{2+}$ desolvation and ionic migration on NC with/without SANi.

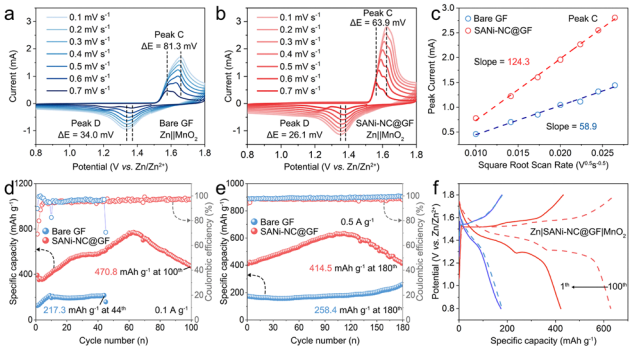

Fig. 4 (a) and (b) CV curves of Zn|GF|MnO_2 with/without SANi-NC. (c) I_p slope chart. (d) Long-cycle tests of Zn|GF|MnO_2 with/without SANi-NC under a current density of (d) 0.1 A g^{-1} and (e) 0.5 A g^{-1}. (f) Charging and discharging curves of Zn|GF|MnO_2 with/without SANi-NC at 0.5 A g^{-1}.

within $Zn(H_2O)_6^{2+}$ (Fig. 3e). Coupled with the rapid electron conduction of NC, the desolvation of $Zn(H_2O)_6^{2+}$ is greatly promoted, liberating massive free Zn^{2+}.[34] Meanwhile, fast Zn^{2+} transport and decreased residual interfacial active H_2O jointly contribute to highly stable and high-performance Zn‖MnO_2 batteries.[35]

Subsequently, SANi-NC@GF served as a functional separator in Zn‖MnO_2 cells to accelerate interfacial Zn^{2+} transport kinetics.[36] As shown in Fig. S5, benefiting from the optimized regulation of interfacial ion transport, the SANi-NC@GF-based Zn‖MnO_2 cell delivers reduced interfacial impedance, laying a foundation for outstanding electrochemical performance. Cyclic voltammetry (CV) measurements at various scan rates were carried out for Zn|GF|MnO_2 cells with/without SANi-NC (Fig. 4a and b). Within the initial CV curves recorded at scan rates ranging from 0.1 to 0.7 mV s^{-1}, the voltage gaps between oxidation (peak C) and reduction (peak D) peaks of the cell with bare GF reach 81.3 mV and 34.0 mV, respectively, considerably larger than those of the SANi-NC@GF-based cell (63.9 mV and 26.1 mV, respectively). This phenomenon originates from the presence of partially desolvated $Zn(H_2O)_x^{2+}$ at the interface, which induces sluggish ionic transport and leads to competitive embedding of active H_2O, resulting in severe electrochemical hysteresis, especially during the charging process.[37] Furthermore, the slope derived from plotting peak current (I_p) against the square root of scan rate provides straightforward insight into interfacial ionic diffusion behaviors. As shown in Fig. 4c and Fig. S6, the Zn|SANi-NC@GF|MnO_2 cell exhibits much higher I_p values for both peak C and peak D (124.3 and 57.1), further verifying accelerated interfacial ionic diffusion kinetics. Galvanostatic charge/discharge tests were further performed to confirm the catalytic effect of SANi-NC on full cell performance. Under a current density of 0.1 A g^{-1}, the bare Zn|GF|MnO_2 cell suffers severe capacity decay, retaining only 217.3 mAh g^{-1} after 44 cycles (Fig. 4d). In contrast, benefiting from the optimized Zn^{2+} transport kinetics enabled by SANi-NC, the cell maintains a high discharge specific capacity of 470.8 mAh g^{-1} over 100 cycles. What's more, under a higher current density of 0.5 A g^{-1}, the strong electric field partially weakens the interfacial desolvation capability. Thus, the Zn|SANi-NC@GF|MnO_2 cell still retains a capacity of 414.5 mAh g^{-1} after 180 cycles (Fig. 4e). Notably, due to interfacial activation and the construction of fast ion transport pathways, the discharge specific capacity of the cell with SANi-NC@GF gradually rises in the early cycling stage, increasing from 411.2 mAh g^{-1} (1st cycle) to 622.8 mAh g^{-1} (100th cycle, Fig. 4f). By contrast, the bare GF-based cell maintains a persistently low discharge capacity throughout the electrochemical reactions due to the absence of efficient ionic transport channels and continuous interfacial degradation.

In summary, SANi-NC serves as an interfacial ionic kinetic regulator to realize rapid desolvation of $Zn(H_2O)_6^{2+}$ at the cathode–electrolyte interface, thereby accelerating reactions. Theoretical calculations demonstrate that the atomic SANi active sites can firmly anchor H_2O (0.17 eV), propel interfacial charge transfer, and simultaneously reduce the desolvation barrier of $Zn(H_2O)_6^{2+}$ (1.80 eV) and the diffusion barrier of Zn^{2+} (0.06 eV). As a result, the Zn|SANi-NC@GF|MnO_2 cell retains a high specific capacity of 470.8 mAh g^{-1} after 100 cycles at 0.1 A g^{-1}. This work offers a novel strategy for developing high-performance Zn‖MnO_2 batteries by utilizing single-atom stepwise catalytic desolvation.

Conflicts of interest

There are no conflicts to declare.

Data availability

The data supporting this article have been included in the main text and the supplementary information (SI). Supplementary information: experimental details, materials and reagent information, and XPS, DFT, and interfacial impedance results. See DOI: https://doi.org/10.1039/d6cc04776a.

Acknowledgements

Dr Jian Wang acknowledges the fellowship support provided by the Alexander von Humboldt Foundation. The authors acknowledge financial support from the National Natural Science Foundation of China (No. 22309144), the Natural Science Foundation of Jiangsu Province (BK20210130 and BK20251840), an open funding from the Key Laboratory of Engineering Dielectrics and Its Application (Harbin University of Science and Technology) (No. KFM202507, Ministry of Education), and the Open Project of Inner Mongolia Engineering Research Center of Lithium-Sulfur Battery Energy Storage (No. MDK2025071).

References

1 X. Zhang, Q. Tang, H. Luo, Y. Xu, S. Miao, S. Zhou, C. Xu, Y. Jia, Q. He, J. Peng, L. He, Y. Song, Y. Zhang and W. Cai, *J. Am. Chem. Soc.*, 2025, **147**, 39440–39451.
2 Y. Yang, H. Yang, R. Zhu and H. Zhou, *Energy Environ. Sci.*, 2023, **16**, 2723–2731.
3 H. Yang, R. Zhu, P. He, C. Zhu, S. Kitano, Y. Aoki, H. Habazaki and H. Zhou, *Angew. Chem., Int. Ed.*, 2026, **65**, e1269101.

4 Y. Chen, S. Gu, S. Wu, X. Ma, I. Hussain, Z. Sun, Z. Lu and K. Zhang, *Chem. Eng. J.*, 2022, **450**, 137923.
5 Z. Hu, Z. Han, H. Liu, X. Jiang, K. Bai, S. Huang, Z. Yang, M. Ye, Y. Tang, Y. Zhang, X. Liu, Z. Wen, H. S. Park and C. C. Li, *J. Am. Chem. Soc.*, 2025, **147**, 46632–46641.
6 S. Cheng, X. Cheng, L. Li, Y. Wang, J. Zhang, Y. Zhang, H. Lin and J. Wang, *Adv. Funct. Mater.*, 2026, **36**, e76179.
7 X. Ge, Z. Peng, Q. Zhang, J. Zhu, N. Zhao, Z. Zhang, W. Meng, B. Li, L. Wang, H. Tian, L. Dai and Z. He, *J. Mater. Sci. Technol.*, 2025, **219**, 10–18.
8 D. Chao, W. Zhou, C. Ye, Q. Zhang, Y. Chen, L. Gu, K. Davey and S. Z. Qiao, *Angew. Chem., Int. Ed.*, 2019, **58**, 7823–7828.
9 W. Li, J. Zhang, B. Zhang, K.-L. Zhou and H. Wang, *Chem. Eng. J.*, 2026, **532**, 174620.
10 W. Li, Q. Fei, J. Zhang, B. Zhang, K. L. Zhou and H. Wang, *Adv. Funct. Mater.*, 2026, **36**, e76123.
11 H. Yang, Y. Yang, W. Yang, G. Wu and R. Zhu, *Energy Environ. Sci.*, 2024, **17**, 1975–1983.
12 J. Xu, Q. Dai, R. Yang, Y. Yu, X. Song, D. Wang, L. Zhu, X. Chu, Y. Cao and Y. Wang, *Adv. Mater.*, 2026, **38**, e73355.
13 L. Jia, H. Hu, X. Cheng, H. Dong, H. Li, Y. Zhang, H. Zhang, X. Zhao, C. Li, J. Zhang, H. Lin and J. Wang, *Adv. Energy Mater.*, 2023, **14**, 2304010.
14 S. Tang, J. Li, T. Wang, T. Wang, W. Xiang, Y. Xiao, H. M. Park, S. Xu, J. S. Yu and H. Pang, *Nat. Commun.*, 2026, **17**, 8463.
15 J. Wang, B. Tang, J. Wu, J. Zhang, Z. Cao, H. Li, Y. Miao, H. Li, F. Wu, F. Liu, D. Wang, Y. Zhang, Q. Xiao, H. Lin and M. Fichtner, *Sci. Adv.*, 2026, **12**, eaef9111.
16 H. Liu, X. Jiang, Z. Hu, Z. Han, J. Chen, K. Bai, Y. Zhang, W. Du, M. Ye, Y. Tang, X. Liu, Z. Wen and C. C. Li, *Adv. Mater.*, 2025, **37**, 2509622.
17 J. Wang, J. Zhang, X. Cheng, Y. Zhang, H. Li, Q. Guan, F. Wu, H. Li, D. Wang, M. Liu, Y. Zhang, Q. Xiao, S. Passerini and H. Lin, *J. Am. Chem. Soc.*, 2025, **147**, 44633–44651.
18 J. Wang, J. Zhang, Y. Zhang, H. Li, P. Chen, C. You, M. Liu, H. Lin and S. Passerini, *Adv. Mater.*, 2024, **36**, 2402792.
19 X. Cheng, W. Wang, Z. Tang, Y. Zhang, B. Chen, J. Zhang, F. Ye, J. Dong, H. Li, J. Jia, Q. Xiao, H. Lin and J. Wang, *Angew. Chem., Int. Ed.*, 2026, **65**, e22417.
20 X. Cheng, Y. Zuo, Y. Zhang, X. Zhao, L. Jia, J. Zhang, X. Li, Z. Wu, J. Wang and H. Lin, *Adv. Sci.*, 2024, **11**, e2401629.
21 Y. Du, Y. Wang, B. Yang, X. Liu, C. Li, W. Li, P. Zhang, H. Lu, D. Bin and Y. Xia, *Nano Lett.*, 2025, **25**, 1002–1009.
22 Z. H. Che, Y. Z. Zhang, J. Wang, B. S. Liu, Y. H. Lin, Z. Y. Wang, H. Wang, D. Bin, H. B. Lu, B. B. Yang, H. B. He, H. Z. Lin, J. Zhang, Y. L. Wang and L. Zhan, *J. Phys. Chem. Lett.*, 2026, **17**, 4879–4890.
23 F. Na, X. Li, J. Wang, X. Cheng, J. Zhang, Y. Wang, H. Lin, L. Zhan, L. Ling and Y. Zhang, *Energy Storage Mater.*, 2025, **78**, 104228.
24 Z. Wu, Y. Zuo, Y. Zhang, X. Li, J. Zhang, Y. Wang, C. Shen, X. Cheng, M. Liu, H. Liu, H. Lin, J. Wang, L. Zhan and L. Ling, *Energy Storage Mater.*, 2024, **70**, 103463.
25 Q. Tang, X. Zhang, S. Zhou, Y. Xu, L. He, S. Chen, W. Cai and Z. Wei, *Energy Environ. Sci.*, 2025, **18**, 9538–9549.
26 Y. Lin, J. Wang, X. Zhang, X. Cheng, Q. Zhuang, J. Zhang, Q. Guan, Y. Wang, C. Shen, H. Lin, L. Zhan, L. Ling and Y. Zhang, *Adv. Funct. Mater.*, 2025, **35**, 2501496.
27 Z. Wang, X. Yang, G. Zhao, D. Wang and Y. Chen, *Energy Environ. Mater.*, 2026, **9**, e70300.
28 Z. He, X. Zhu, Y. Song, B. Li, X. Xu, Z. Zhang, N. Zhao, Y. Liu, J. Zhu, L. Wang, L. Dai and H. Tian, *Energy Storage Mater.*, 2025, **74**, 103886.
29 X. Jiao, J. Lei, Z. Huang, Y. Zuo, Z. Zhuang, Y. Luo, J. Qi, Z. Wang, L. Lu, W. Yan and J. Zhang, *Adv. Funct. Mater.*, 2025, 35.
30 Z. Wang, X. Yang, G. Zhao, D. Wang and Y. Chen, *Nano Res.*, 2026, **19**, 94908560.
31 J. Zhang, F. Liu, R. He, Q. Guan, N. Tian, J. Wu, Z. Cao, S. Yin, Y. Zhang, L. Jia, X. Li, C. You, H. Liu, M. Liu, Y. Miao, H. Lin and J. Wang, *Adv. Mater.*, 2026, **38**, e10894.
32 X. Zhang, Q. Tang, H. Luo, W. Xie, B. Wang, S. Zhou, S. Cao, L. Wang, Q. He, J. Peng, X. Yan, T. Chen and W. Cai, *Adv. Energy Mater.*, 2025, **16**, e04638.
33 X. Zhao, J. Wang, X. Cheng, H. Hu, J. Zhang, J. Wu, F. Liu, S. Cheng, Q. Guan, Y. Zhang, A. Naveed, Y. Liu, H. Lin, J. Wu and J. Lu, *Adv. Funct. Mater.*, 2025, **36**, e22711.
34 J. Dong, X. Cheng, H. Yang, H. Li, H. Liu, L. Jia, Y. Zhang, Q. Guan, J. Jia, F. Wu, J. Zhang, M. Liu, H. Lin and J. Wang, *Adv. Mater.*, 2025, **37**, 2501079.
35 G. Wu, R. Zhu, W. Yang, Y. Yang, J. Okagaki, Z. Lu, J. Sun, H. Yang and E. Yoo, *Adv. Funct. Mater.*, 2024, **34**, 2316619.
36 Y. Song, P. Ruan, C. Mao, Y. Chang, L. Wang, L. Dai, P. Zhou, B. Lu, J. Zhou and Z. He, *Nano-Micro Lett.*, 2022, **14**, 218.
37 H. Yang, R. Zhu, Y. Yang, Z. Lu, Z. Chang, P. He, C. Zhu, S. Kitano, Y. Aoki, H. Habazaki and H. Zhou, *Energy Environ. Sci.*, 2023, **16**, 2133–2141.

